Electronic Supplementary Material (ESI) for Sustainable Energy & Fuels.

Supporting Information for:

Unravelling the practical solar charging performance limits of redox flow battery based on the single photon device system

Dowon Bae,†,* Gerrit M. Faasse,† Gerasimos Kanellos, Wilson A. Smith*

Delft University of Technology, Department of Chemical Engineering - Materials for Energy Conversion and Storage (MECS), Delft 2600GA, The Netherlands

**Corresponding author – d.bae@tudelft.nl; w.smith@tudelft.nl*

†*These authors contributed equally*

S1. Detailed working conditions and performance for the references in Figure 1

Table S1. Working conditions (Photo-absorber, band-gap, Redox couples, Redox potential, etc.) and STC efficiencies

Ref. #	Ref. # (ESI)	Photo-absorber	E_g, eV	Redox couples (Anolyte$\Vert$Catholyte)	Optical path length	Cell volume, mL	E_{Redox}, V	STC%	Remark
19	1	c-Si (p-type base)	1.12	$Fe(CN)_6^{3-/4-}\Vert TEMPO\text{-}Sulfate^{+/0}$	2 mm	6	0.35	1.8	
22	2	n-WSe_2 (crystalline)	1.2	$I_3^-/I^-\Vert AQS/AQSH_2$	1 mm	4	0.51	3.9	
24	3	n-Fe_2O_3	2.2	$Fe(CN)_6^{3-/4-}\Vert AQDS^{0/2-}$	5 mm	Unknown	0.74	0.02	
27	4	n-WSe_2	1.4	$I_3^-/I^-\Vert AQ/AQH_2$	1 mm	15	0.62	5.1	He-Ne laser (150 mW·cm^{-2})
31	5	n-$BiVO_4$	2.4	$I_3^-/I^-\Vert Br_3^-/Br^-$	none	0.05	0.55	1.6	Back-side illuminated
30	6	DSSC (Z907)	2.0	$I_3^-/I^-\Vert AQDS/AQDSH_2$	none	Unknown	0.28	0.5	Back-side illuminated TiO_2 scaffold layer
29	7	n-$MoSe_2$ (crystalline)	1.3	$Br_2/Br^-\Vert I_2/I^-$	Unknown	2	0.58	0.5	200 mW·cm^{-2}
29	7	n-GaAs	1.42	$Se_2^{2-}/Se^{2-}\Vert Cd^{2-/0}$	Unknown	2	0.30	2.8	
29	7	n-CdSe	1.74	$S_n^{2-}/S^2\Vert Se_2^{2-}/Se^{2-}$	Unknown	2	0.11	0.3	
29	7	n-CdSe	1.74	$S_n^{2-}/S^{2-}\Vert Cd^{2-/0}$	Unknown	2	0.35	0.8	
This work	n/a	c-Si (n-type base)	1.12	$Br_2/Br^-\Vert Fe(CN)_6^{3-/4-}$	none	20	0.61	3.2	Back-side illuminated

S2. Theoretical calculations

Molar absorptivity (ε)

The molar absorptivity, used to calculate the parasitic absorption by the electrolyte, can be approximated by the Beer-Lambert law from the measured absorbance (*A*):

$$\varepsilon = \frac{A}{c \cdot l} \quad (1)$$

where A is absorbance, c and l are the concentration and thickness of the electrolyte, respectively.

Solar flux (Φ)

Losses due to both reflection and parasitic absorption are considered by including their effects on the absorbed solar flux (and consequently on $j_{max,ph}$) using the following equation:

$$\Phi_{abs} = \Phi_{AM1.5} \cdot T_{el} \cdot \left(1 - R_{ph}\right) \quad (2)$$

in which Φ_{abs} is the absorbed solar flux, $\Phi_{AM1.5}$ is the incident solar flux, T_{el} is the transmission spectrum for the electrolyte, which can be derived from the measured *A* using the Beer-Lambert law, and R_{ph} is the total reflectance spectrum of the device).

Absorption probability (Abs)

To account for photons escaping the photo absorber after multiple reflections, the absorption probability spectrum of the semi-conductor is found using the Tiedje-Yablonovitch-limit[8]:

$$Abs = \frac{\alpha(\lambda)}{\alpha(\lambda) + \dfrac{1}{4n(\lambda)^2 d}} \quad (3)$$

in which $\alpha(\lambda)$ is the absorptivity spectrum and d is the thickness of the photo-absorber (350 μm in this work).

S3. Back-illuminated photoelectrode preparation method

Silicon-based photoelectrode

The thickness of the n-type CZ c-Si wafer was 350 µm ([100]; Topsil, 1–20 ohm·cm). The shallow np$^+$-junction was produced in n-type Si wafer by thin p$^+$ doping using an atmospheric pressure tube furnace in close proximity with BoronPlus planar diffusion sources. The temperature was ramped up to 950˚C at a rate of 10 ˚C/min in 0.1 SLM oxygen and 8 SLM nitrogen. The boron phase-layer was removed by dipping the wafers in a buffered HF bath for 5 min. Then the dopant on the backside (unpolished) of the wafer was removed by etching in a reactive ion etching (RIE) process (Pegasus, SPTS Technologies). 3 µm tall mesas on the front of the wafer were defined by UV lithography followed by a 3 µm deep RIE etch.

Conducting layer formation

Thin films of 2-nm-thick Pt were prepared at room temperature with reactive sputter deposition on np$^+$-Si. The deposition rate was calibrated with an in-chamber QCM (quartz crystal microbalance). A ring-shaped Au layer was deposited on the p$^+$-Si surface using a reactive sputtering with a home-made metallic mask at room temperature. The surface was cleaned with Ar-sputtering in vacuum to remove the native oxide layer. In the case of Pt on the n-type surface, the surface has been etched chemically in KOH bath for an hour prior to the Ar-cleaning for flattening of the rough surface.

For the electrochemical experiment under the dark, various conducting layers, including the Pt, were deposited onto highly-doped n$^+$-Si substrates for Figure 4d in the main manuscript. The carbon was sputtered at room temperature or 400˚C. In the case of the TiO_2, a thin layer of titanium was sputtered on first to prevent silicon oxidation in the subsequent TiO_2 reactive sputtering step at 400˚C as described elsewhere.[1,9]

Chemicals for electrolyte

The synthesis of TEMPO-4-sulfate was based on previous studies.[1,10] 4-Hydroxy- TEMPO (Henan Tianfu Chemical Co. LTD, >99%) was added to concentrated H_2SO_4 (Sigma Aldrich 97%) at a molar ratio of 0.044. The solution reacted at room temperature for 20 min and dripped slowly into a suspension of $NaHCO_3$ (Sigma-Aldrich) resulting in a neutral, yellow solution. The solution was shaken with ethyl acetate (Sigma-Aldrich) and the ethyl acetate phase was discarded, before concentrating the aqueous solution of the reaction product at 50˚C using a rotary evaporator. And then acetone was added to precipitate Na_2SO_4. The acetone phase was then evaporated using a rotary evaporator again, and the resulting red/orange salt was used without further purification.

$K_3Fe(CN)_6$ (Sigma-Aldrich, >99%) and NH4Br (Sigma-Aldrich, >99.99%) were used as received after mixing with 1M NH_4Cl to make a 0.4M $Fe(CN)_6^{3-}$ catholyte and 0.4M Br^- anolyte, respectively. AQS(2) (Sigma-Aldrich, 98%) was also used without further treatment with 1M H_2SO_4 (Sigma-Aldrich) to make a catholyte used for the GaP device.

Characterization

The PEC charging measurement in Fig. 3f has been done in ferri/ferrocyanide electrolyte solution (in 1M NH_4Cl) which has been adjusted to pH 7 by the addition of NH_4OH. A PARSTAT MC potentiostat (Princeton Applied Research, AMETEK) and a Hg/$HgSO_4$ reference electrode were used for all electrochemical measurements.

The solar charging has been done under simulated AM1.5 solar irradiation (100 mW·cm^{-2}) using a Newport Sol3A Class AAA solar simulator with a 450W Xenon short arc lamp. The solutions were purged with nitrogen before and during measurements.

The absorbance and reflectance spectra were recorded by using a PerkinElmer-Lambda 900 UV-Vis spectrometer to estimate the parasitic absorption by the electrolyte and reflection loss at the sample surface. To avoid the effect of the background signal, a baseline correction was carried out prior to the measurements

S4 Contour plots for various electrolytes in front lit configuration

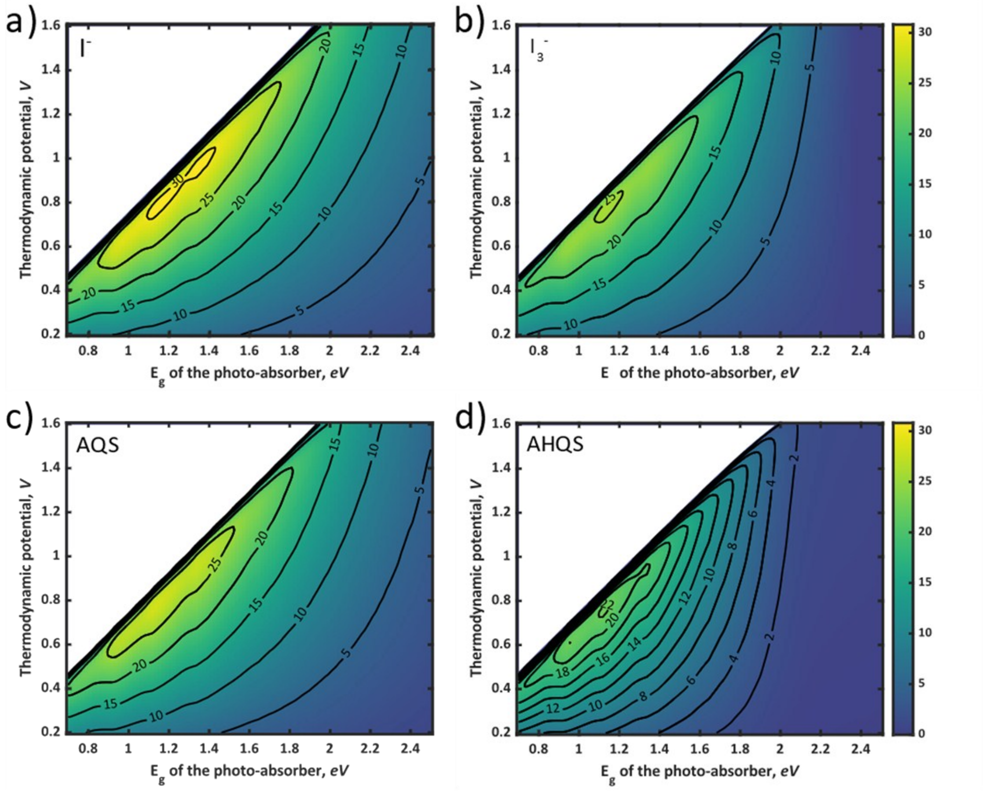

Figure S1. Contour-plots for I^- (a), I_3^-(b), AQS (c) and AHQS (d) in front lit configuration, showing the sensitivity of the STC for the electrolyte absorption. Note that in general the absorption spectrum of the redox species in the couples (e.g., I^-/I_3^-) are different, meaning that the parasitic electrolyte absorption (and thus the STC) depends on the SOC of the battery.

S5. Reflection spectra for silicon photo absorber in different cases

In figure S2a and b, the schematic depictions of the front- and backlit setups and the reflection spectra of silicon in different cases, show an explanation as to why there are situations in which front-side illumination outperforms back-side illumination, as seen in Figure 3e of the main paper (which is counter-intuitive at first glance). It is seen that the reflection of the silicon is higher when the light is coming from the air, as opposed to when it is coming from an electrolyte. In this way, the electrolyte acts as an antireflective layer, as seen in Figure

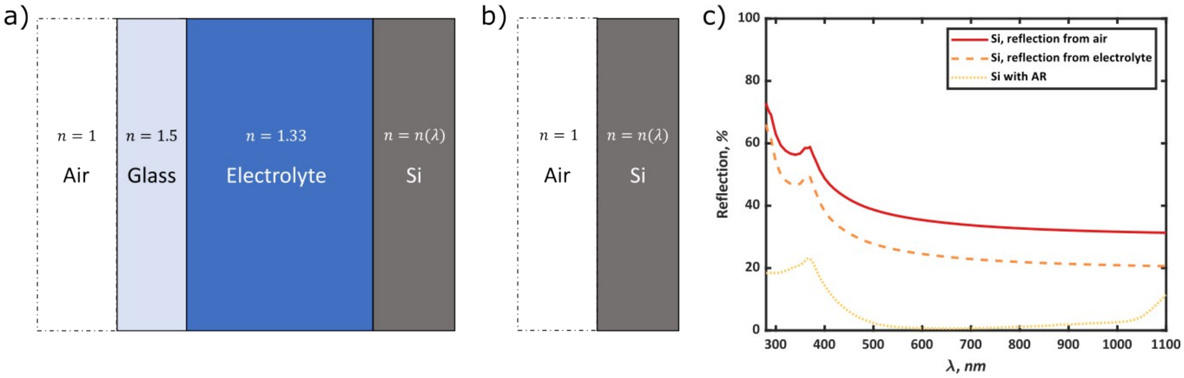

Figure S2. In a and b, schematic representations of the reflection interfaces are shown in case of front-lit (a) and back-lit (b) configurations. In c, three reflection spectra of silicon are shown: reflection of bare silicon when lighting from air, reflection of bare silicon when lighting from an electrolyte and the reflection of AR-treated silicon. Since the refractive index of the electrolyte is closer to that of the

S2c), and this effect could outweigh the electrolyte absorption. This results in some front-lit configurations outperforming back-side illumination.

S6. Electrolyte resistance example calculation

To calculate the total resistance of an electrolyte, consisting of an 1M NH_4Cl supporting electrolyte and an active redox electrolyte with an estimated specific conductivity of 75 mS/cm, the NH_4Cl curve in Figure 5c) of the original paper is linearly interpolated to find a specific conductivity of 101.2 mS/cm. Using the specific conductivity of 75 mS/cm for the active electrolyte, the total conductivity is approximated by 75+101.2 = 176.2 mS/cm (Kohlrausch's law of independent ionic migration). In this work, interionic interactions are not considered. The resistance can be calculated using:

$$R \cdot A = \frac{l}{\kappa} = \frac{2}{0.1762} \approx 11.35 \ \Omega \cdot \text{cm}^2 \qquad (4)$$

with l the path-length, A the area and κ the conductivity. The other resistances are calculated in the same manner.

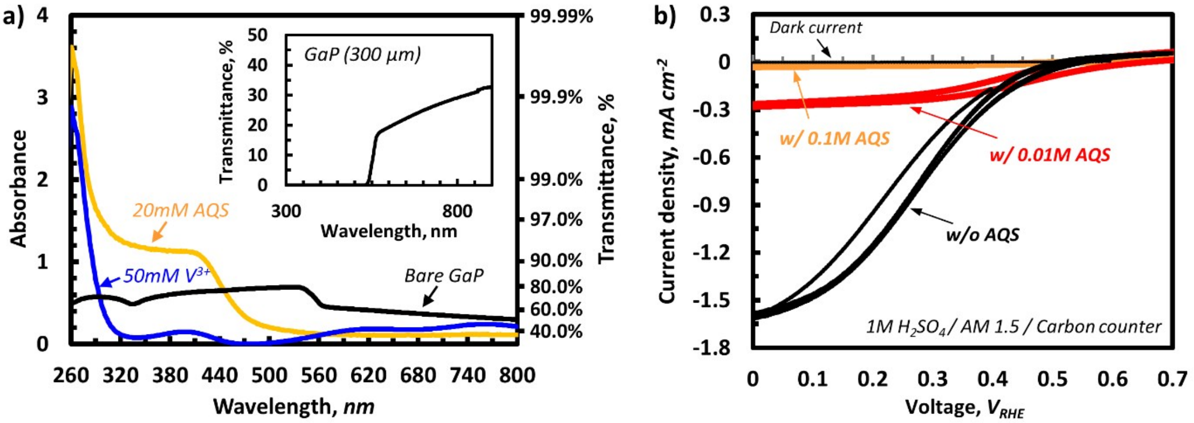

Figure S3. Experimental absorption spectra of AQS, vanadium (III) and GaP (300 µm thick) wafer (a). The inset shows transmittance data measured using a UV-Vis to derive absolute absorbance data of the GaP sample. (b) shows the impact of AQS addition into the sulfuric acid electrolyte on the cathodic reaction of the GaP device under the light.

S7. Absorption spectrum and cyclic voltammetry of GaP device

S8. Two-electrode charging/discharging experiments

1 K. Wedege, D. Bae, E. Dražević, A. Mendes, P. C. K. Vesborg and A. Bentien, *RSC Adv.*, 2018, **8**, 6331–6340.

2 J. R. McKone, F. J. DiSalvo and H. D. Abruña, *J. Mater. Chem. A*, 2017, **5**, 5362–5372.

3 K. Wedege, J. Azevedo, A. Khataee, A. Bentien and A. Mendes, *Angew. Chemie - Int. Ed.*, 2016, **55**, 7142–7147.

4 B. Keita and L. Nadjo, *J. Electroanal. Chem.*, 1984, **163**, 171–188.

5 Y. Zhou, S. Zhang, Y. Ding, L. Zhang, C. Zhang, X. Zhang, Y. Zhao and G. Yu, *Adv. Mater.*, 2018, **30**, 1–7.

6 W. D. McCulloch, M. Yu and Y. Wu, *ACS Energy Lett.*, 2016, **1**, 578–582.

7 P. G. P. Ang and A. F. Sammells, *Faraday Discuss. Chem. Soc.*, 1980, **70**, 207–222.

8 T. Tiedje, E. Yablonovitch, G. D. Cody and B. G. Brooks, *IEEE Trans. Electron Devices*, 1984, **31**, 711–716.

9 D. Bae, T. Pedersen, B. Seger, M. Malizia, A. Kuznetsov, O. Hansen, I. Chorkendorff and P. C. K. Vesborg, *Energy Environ. Sci.*, 2015, **8**, 650–660.

10 J. Winsberg, C. Stolze, A. Schwenke, S. Muench, M. D. Hager and U. S. Schubert, *ACS Energy Lett.*, 2017, **2**, 411–416.

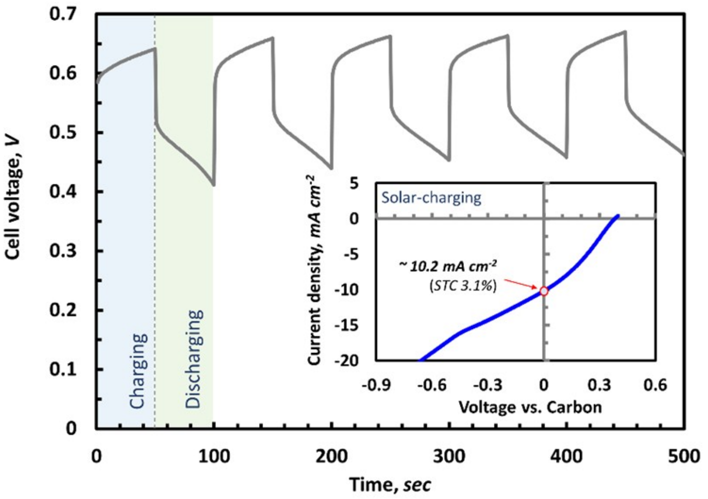

Figure S4. Charge/discharge curves in a RFB cell (Redox-flow.com) with a 25 cm^2 active area at constant current density of 3.2 mA cm^2 and electrolyte concentration 0.4M ferrocyanide and 0.4M NH_4Br in 1M NH_4Cl. The inset shows the LSV of 2-electrode cell under 100 mW·cm^{-2} light using a same electrolyte condition resulting in a current density of 10.2 mA·cm^{-2}.